WING PROFILE INVESTIGATIONS IN THE LOW SPEED WIND TUNNEL OF THE UNIBWM

O Meyer[1]*, T Terreblanche[2], M Klein[2]
[1]Universität der Bundeswehr München, Dept. of Mechanical Engineering, Germany
[2]TEG Tubercle Engineering Group GmbH, Munich, Germany

Abstract

The experimental environment in the low speed wind tunnel was optimized to perform 2D airfoil polar tests in an open test section. The streamwise axial static pressure gradient in the test section was minimized, given airfoil models were installed in the test section and the lift and drag measurement procedures were optimized. The test setup was validated by the comparison of clean-case airfoil results with reference data from other wind tunnels. The measurement of a profile polar, including model exchange, has been reduced to less than one hour. The obtained setup was implemented in the investigation of the effect of various leading edge modifications on the high lift behavior of two given wind turbine profiles. Leading edge tubercle as well as DLR LEVoG variations were investigated in order to limit the lift production of the airfoils at angles of attack beyond the wind power plant's operation point. It is shown, that the lift gradient at higher angles of attack can be reduced and additional drag can be kept to a minimum with particular tubercle and LEVoG configurations.

1. INTRODUCTION

1.1. Motivation

In Germany during the winter of 2016/17, several wind turbines suffered severe damages due to heavy wind gusts experienced from stormy weather conditions. The existing mechanical safety systems were not capable of preventing these damages and is assumed to be the result of delayed reaction times. One idea to improve the mechanical integrity of wind turbines in gusty conditions is to use airfoils with limited high lift capacities beyond the designed operation point. I.e. the aerodynamics of the airfoil itself should limit the wing load directly in critical wind conditions.
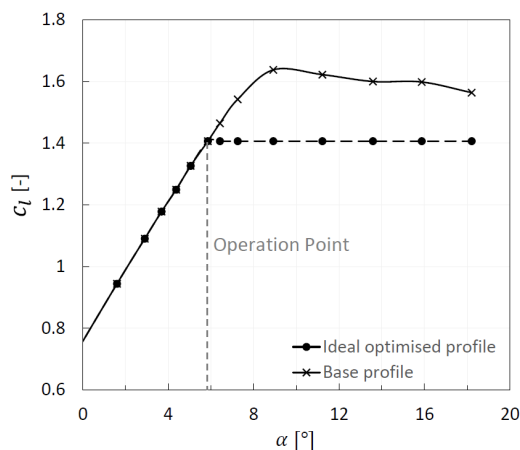

FIGURE 1. Lift polar of base profile (solid) and targeted lift polar for safer wind turbine operation (dashed).

An ideal behavior of such a profile is illustrated in FIGURE 1. The solid lift polar represents a standard base airfoil with typical high lift characteristics. The operation point may be at appr. 6° angle of attack, whereas the lift rises further up to 10° angle of attack. The dashed curve depicts an ideal behavior of a high lift limited wind turbine airfoil, which will have a constant lift at angles of attack above the operation point. The challenge is to design profiles with such characteristics or to develop measures which can be retrofitted to existing wind turbine blades for safe operation.

1.2. Tubercle Technology

One promising approach may be the use of so called leading edge tubercles which could be applied to the leading edges of airfoils to influence the high lift characteristics. The idea was formulated by F.E. Fish and J.M. Battle in [1] in which they investigated the morphology of humpback whale flippers, see FIGURE 2. The leading edge tubercles were suspected to support the whale's maneuverability and hence the high lift requirements of the flippers at higher angles of attack.

Later wind tunnel experiments with flipper models proved this hypothesis [2] and showed that tubercles can delay stall to higher angles of attack and may additionally result in a higher lift at increased angles of attack. Where this effect was observed for the investigated test case and flipper models, the effect of tubercles differed for infinite wing models, i.e. 2D airfoils. It was shown for example in [3] and [4] that tubercles may limit the lift beyond the design point and show the desired characteristics depicted in FIGURE 1 with additional higher post stall lift at very high angles of attack compared to the baseline profile without tubercles.

However, other research showed, that the aerodynamic effect of tubercles depend on various parameters such as Reynolds number, baseline profile, 2D or 3D flow (finite or infinite wing, wing shape), amplitude, wavelength and shape of the tubercles etc. as indicated for example in [5], [6], [7] and [8].

Therefore, the tubercle technique may represent a promising option to design the required airfoil characteristics as shown in FIGURE 1 but a successful design must be adjusted to the individual boundary conditions for each application.

FIGURE 2. Pectoral fins of a humpback whale with leading edge tubercles, detail of photograph taken by Christopher Michel and used under CC license from flickr.

1.3. LEVoG Technology

Another approach identified is the use of Leading Edge Vortex Generators (LEVoGs), which were first developed by Geissler, Dietz, Mai and Richard in [16] as a passive dynamic-stall control device by means of miniature, low aspect ratio vortex generators added to the airfoil leading edge, see FIGURE 3.

Wind tunnel investigations with the rotary aircraft profile OA209 in [16] and [17] showed that due to the LEVoGs location in or near the stagnation point, the flow over the airfoil upper surface remained unaffected at lower angles of attack, only forming small longitudinal vortices and affecting the lift production at higher angles of attack. It was shown in [18] and [19] that the use of low aspect ratio cylindrical LEVoGs, which induced an upward facing velocity, exhibited a larger influence on the flow due to an increased wake height. It was also concluded that for an improved dynamic-stall effect the LEVoG height should be slightly larger than the boundary layer thickness.

These investigations as well as the optimum LEVoG configurations defined in [17] however, mainly focused on the improvement of dynamic stall conditions. Therefore, further research is needed to optimize LEVoGs for the use in wind turbine applications, in which a limited lift production after the operation point as shown in FIGURE 1 is desired. Since the aerodynamic effect of the LEVoGs also depends on various parameters such as Reynolds number, baseline profile, height H, diameter D, distance to the airfoil leading edge s as well as the spacing between the LEVoGs S, the LEVoG design must also be adjusted to the individual boundary conditions for each application.
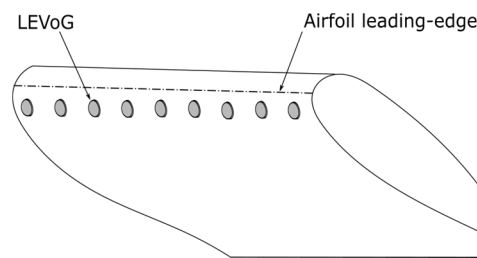

FIGURE 3. Drawing of an airfoil with Leading Edge Vortex Generators (LEVoGs), [11].

2. WIND TUNNEL OF THE UNIVERSITÄT DER BUNDESWEHR MÜNCHEN (UNIBWM)
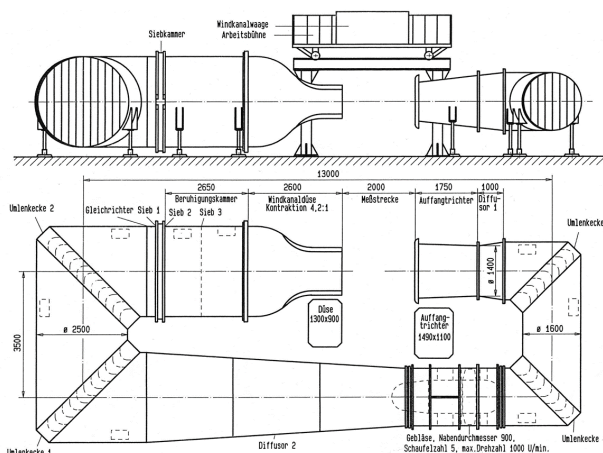
2.1. Overview and Technical Data

FIGURE 4. Wind Tunnel of the UniBwM, Department of Mechanical Engineering

Test Section (h x w x l)	0,9 m x 1,3 m x 2 m
Velocity	0 - 40 m/s
Test Section Re-nr.	2.8·106
Power	75 kW
Turbulence	0.35%
Ground Simulation (Belt with BL Removal System)	0-40 m/s
Axial Static Pressure Gradient	$\frac{dc_p}{dx} < \frac{0.002}{0.1m}$

TAB 1. Technical data of the used UniBwM wind tunnel.

Component	Range [N]	Res. [N]	Max dev. from value
Drag I	0 - 100	0,1N	0.24%
Drag II	0 - 100	0,1N	0.32%
Lift I	0 - 200	0,1N	0.02%
Lift II	0 - 200	0,1N	0.02%
Lift III	0 - 200	0,1N	0.02%
Lateral	0 - 100	0,1N	0.32%

TAB 2. Technical data of the used UniBwM wind tunnel balance.

2.2. Requirements

The low speed wind tunnel of the Dept. of Mechanical Engineering of the UniBwM had to be prepared in order to investigate existing 2D wing airfoils with different leading edge modifications. The aim was to obtain lift and drag polars over a geometrical angle of attack range from $-20° < \alpha_{geom} < 25°$ at the maximum achievable Reynolds number. The profile models used have a chord length of $c = 0.35$ m and a span of $b_m = 0.8$ m.

Therefore, the aim was to identify and optimize the flow quality in the test section, install the models in the test section, realize a 2D flow, accurately measure the drag and lift, implement test section correctional methods and to validate the obtained setup against reference data. The planned development of airfoils with different leading edge devices can thus be conducted after the successful preparation of the wind tunnel and validation of the reference data.

2.3. Wind Tunnel Optimization and Test Setup

The used wind tunnel was built in 1975 and has undergone several updates since, for example the change from a circular to a rectangular nozzle exit, the implementation of a moving belt for ground effect simulation, the addition of acoustic splitter plates in the airline and a new wind tunnel control system.

The wind tunnel operates with an open test section which can lead to a nonlinear streamwise pressure/velocity distribution due to an accelerated flow from the nozzle exit onwards and a decelerated flow before the collector entry. The non-uniform axial pressure distributions of several ¾ open jet wind tunnels are shown for example in [9]. The UniBwM wind tunnel showed a strong pressure gradient which was optimized by the inclination of the Seiferth wings at the nozzle exit and the application of additional flaps at the collector entry. FIGURE 5 shows the axial static pressure distribution in the centerline of the test section before- (upper lines) and after optimization (lower lines) for two velocities each. The nozzle exit is located on the left and collector entry on the right.
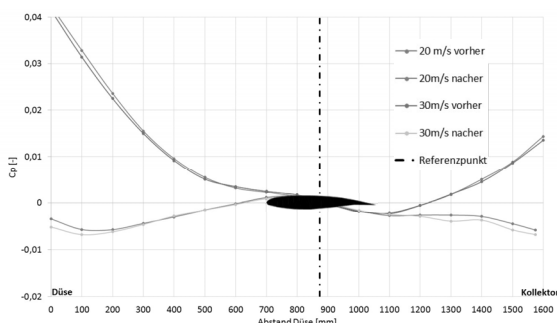

FIGURE 5. Static pressure gradient in test section with model before and after optimization [10].

The turbulence level in the test section was validated via hotwire and pressure sphere measurements and both methods yielded a turbulence level of appr. $Tu = 0.35\%$ in the reference testing position. The maximum testing speed for the entire angle of attack range was limited to 40 m/s

which lead to a testing Reynolds number of appr. $Re = 0.8 \cdot 10^6$ for the given models.

The models were mounted to the overhead balance with the use of circular end plates which have a diameter of twice the model chord to ensure a 2D flow over the airfoil in the open test section.
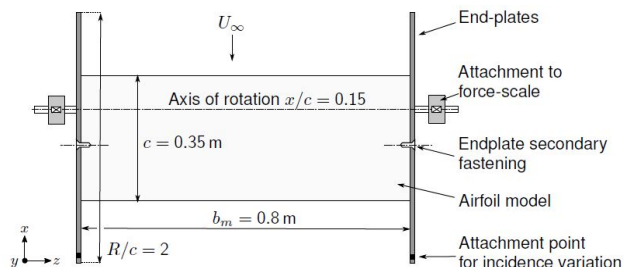

FIGURE 6. Setup of airfoil model in test section, top view [11].

This setup now represents a quasi-open test section with open ceiling and floor. The model blockage was appr. $B = 7\%$ with the end plates and the given model dimensions.

The 2D nature of the airfoil flow was validated with wool tufts on the airfoil surface, surface oil flow technique and infrared thermography [11]. FIGURE 7 shows the 2D nature of the flow visualized with an infrared camera. The small influence of the end plates can be seen as well as a distinct laminar separation and turbulent reattachment line of a laminar separation bubble on the suction side of the airfoil.
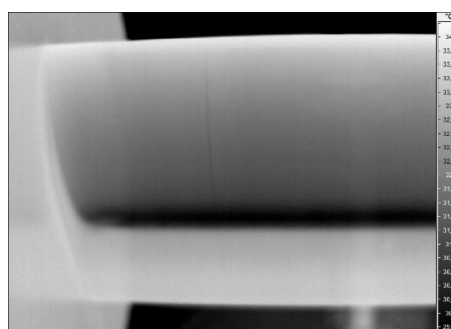

FIGURE 7. Visualization of end plate effects and 2D nature of airfoil flow [11].

2.4. Lift and Drag Determination

The lift forces were directly measured with the overhead wind tunnel balance, which is an AVA-Göttingen type as described in [12]. The technical data are given in TAB 2. The drag forces could not be determined via the wind tunnel balance because the interference drag of the model suspension proved to be too large. Therefore, a wake rake was built with total- and static pressure tubes which was used to derive the profile drag through the analysis of the momentum loss in the wake of the profile. The wake rake was positioned relatively close to the model trailing edge with a distance of $x/c = 0.6$ which required the measurement of both the static- and total pressure in the airfoil wake, [12]. The profile drag c_d was calculated with the formula of Jones [13],

$$c_d = 2 \int\limits_{-\infty}^{\infty} \sqrt{\frac{p_t - p_s}{q_\infty}} \left(1 - \sqrt{\frac{p_t - p_{s,\infty}}{q_\infty}} \right) d\left(\frac{y}{c}\right)$$

where p_t is the local total pressure, p_s the local static pressure in the wake and q_∞ and $p_{s,\infty}$ is the dynamic and static pressure of the undisturbed oncoming flow.

The total pressure can be measured within an accuracy of 1% in a local flow angle regime of ± 7° [14]. A correction for higher angles of attack was determined for the test setup and the planned angle of attack regime via potential flow theory and the Biot-Savart-Law, see [11]. A maximum correction of 5% in total pressure and 8% in static pressure was estimated. The pressures were measured via two PSI µDAQ64 miniature pressure modules.

The used wake rake was a preliminary design which influenced the static measurement and the local angle calibration of the oncoming flow at the pitot- and static tubes was also incomplete. Therefore, a new pitot and new static rake was designed and the angle sensitivity was calibrated to improve future measurements.

3. VALIDATION RESULTS

The validation measurements were performed for two reference laminar wind turbine profiles, TEG4418 and TEG2618 with a clean leading edge. These profiles were to be implemented for the investigation of the tubercles and LEVoGs after successful validation.

The results for the TEG4418 profile from the UniBwM wind tunnel and results from XFOIL calculations were validated against reference wind tunnel data from the Deutsche WindGuard in Bremerhaven and the laminar wind tunnel of the IAG Stuttgart, see FIGURE 8. The results for the TEG2618 profile from the UniBwM wind tunnel and results from XFOIL calculations were validated against reference wind tunnel data from the Deutsche WindGuard only, see FIGURE 9. The reference wind tunnel data was measured at a Reynolds number of $Re = 1.1 \cdot 10^6$ whereas the tests at the UniBwM could only be performed at max. $Re = 0.8 \cdot 10^6$. The turbulence level in the WindGuard tunnel is $Tu < 0.35\%$ and hence a little lower than the turbulence level in the UniBwM wind tunnel. The turbulence level in the laminar wind tunnel of the IAG in Stuttgart is $Tu < 0.02\%$ and hence much lower than the turbulence level in the UniBwM wind tunnel. The XFOIL calculations were performed at $Re = 0.8 \cdot 10^6$ with an adjusted critical amplification factor. For more information about the XFOIL calculation refer to [15].

3.1. Base Airfoils TEG4418 and TEG2618

The lift polars for the reference wind tunnel data, the XFOIL calculations as well as the UniBwM measurements show a very good coincidence in the zero lift angle α_0, the lift gradient and the lift at $\alpha = 0°$ for the TEG4418 airfoil, see FIGURE 8. This also applies to the TEG2618 airfoil for the comparison of the XFOIL data as well as the Windguard and UniBwM wind tunnel results, FIGURE 9. The lift polars deviate at the maximum lift due to growing test section interferences in the UniBwM wind tunnel and differences in the testing Reynolds number. However, the coincidence of the lift polars in the linear range is very promising, since the

intended design changes of the leading edge modifications is expected to act below the maximum lift, see FIGURE 1.

The drag polars show a larger deviation between the reference wind tunnel measurement, XFOIL calculation and UniBwM measurement. The general shape may be comparable, but the absolute values differ. This may also be attributed to the different Reynolds numbers of the reference and UniBwM measurements, the test section interference corrections and the wake measurement itself, see chapter 2.4.
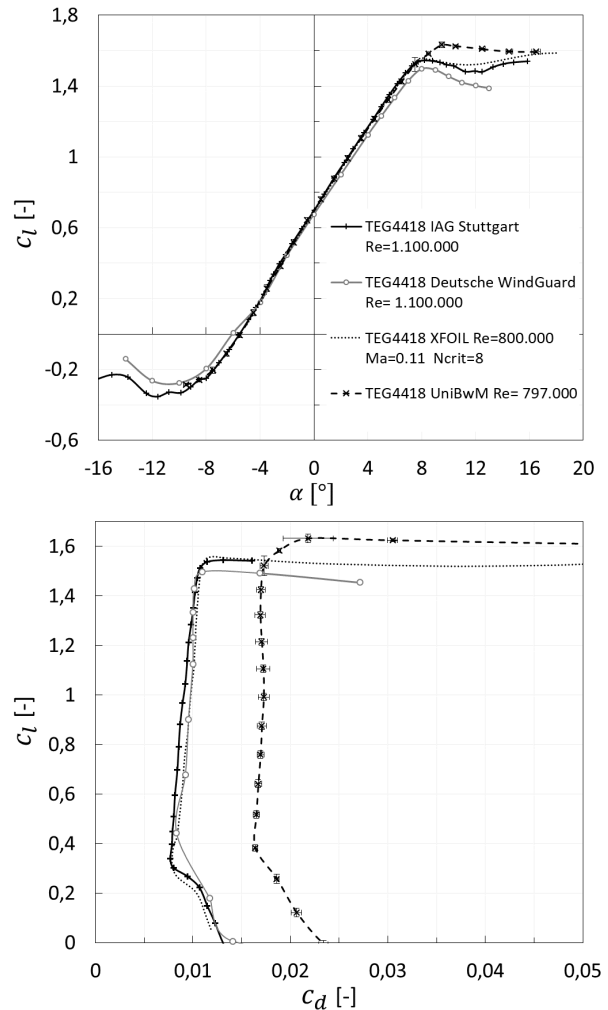

FIGURE 8. Validation polars of the TEG4418 airfoil.

The promising lift polar results in the UniBwM wind tunnel, the fast determination of the polars within 1h including the model exchange and the versatility of the wind tunnel in using optical flow visualization methods lead to the decision to continue with the investigation of leading edge modifications for the two given airfoils.
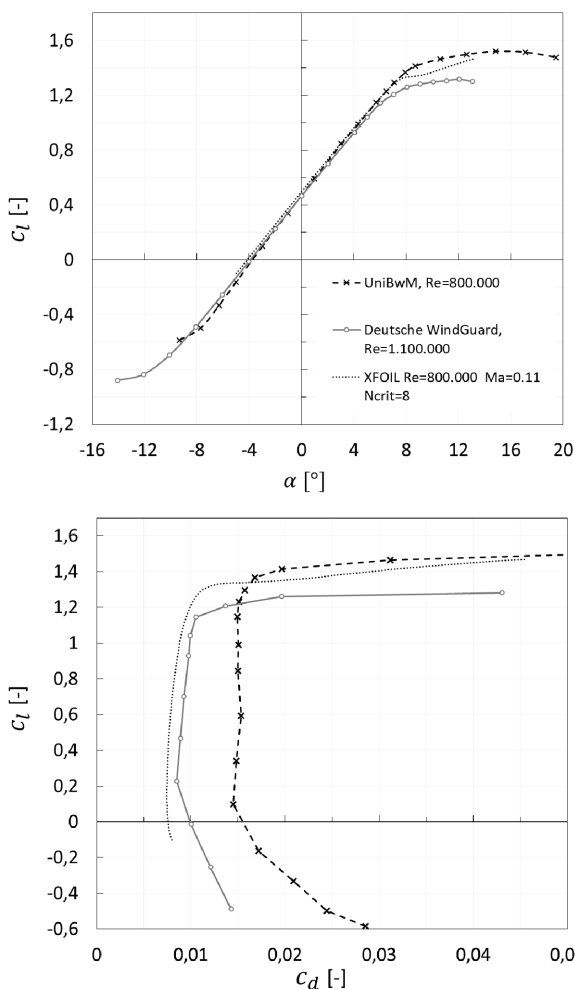
FIGURE 9. Validation polars of the TEG2618 airfoil.

4. LEADING EDGE MODIFICATIONS

In order to obtain the ideal behavior of a high lift limited wind turbine airfoil as illustrated in FIGURE 1, two types of leading edge modifications were investigated namely that of sinusoidal leading edge tubercles and leading edge vortex generators (LEVoGs).

The shape of the tubercles is controlled by the amplitude A, wave length λ as well as the form of the tubercle peaks named V, D and $Disc$, see FIGURE 10. The form V and D indicate the difference in the resulting leading edge radius of the tubercle peaks with the D form implementing a larger radius at the peak and creating a noticeable valley at the trough. The $Disc$ configuration created a plateau at the trough without changing the amplitude or wavelength of the tubercles. Information on the parameter variation is given in TAB 3.

Airfoil	Wavelength λ [%·c]	Amplitude A [%·c]	Form
TEG2618	38	5	V
TEG4418	38	5	V
	38	7.5	V
	38	7.5	D
	38	7.5	$Disc$
	38	10	V
	19	7	V

TAB 3.   Tested tubercle parameter configurations.

The tested LEVoGs were shaped as flat cylinders and a parameter study was conducted for the height H, diameter D, the distance to the leading edge s and for the spanwise spacing S of the LEVoGs, see FIGURE 10. The total ranges tested include: A LEVoG height of $0.14\%·c < H < 0.66\%·c$, LEVoG diameter of $1.14\%·c < D < 2.86\%·c$, distance to the leading edge $0\%·c < s < 2.86\%·c$ and spanwise spacing between the LEVoGs center-to-center of $4.29\%·c < S < 14.29\%·c$.
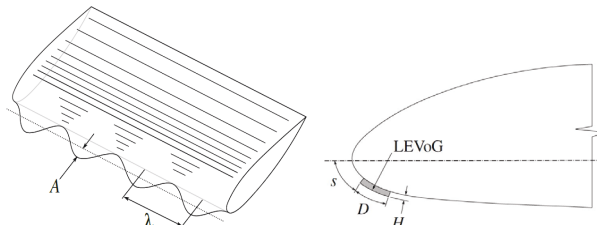

FIGURE 10. Positioning and parameters of tubercles and LEVoGs on an airfoil model, [11].

In order to analyze the influence of the tubercle and LEVoG leading edge modifications, the results of the clean wing case are compared to the results of the various leading edge modifications. The solid line in the resulting figures illustrate the clean wing case with the dashed and dotted lines showing the results for the different tubercle and LEVoG parameter variations.

In order to compare the results of the various modifications, a few analysis criteria are chosen. These criteria are: The angle of attack at which the lift production deviates from the clean wing case, referred to as the activation angle α_{act}, the maximum lift $c_{l,max}$ as well as the ratio of the sum of the drag within the drag bucket of the tested model configuration to that of the clean wing case $c_{d,R}$.

5. TUBERCLE RESULTS

The tubercle variations were tested and the results compared to the clean wing case for the TEG4418 airfoil, tested at a Reynolds number of Re = 8.06·10⁵. As seen from the results, the implementation of the leading edge tubercles does not influence the lift polar at lower angles of attack. As the angle of attack increases the lift production starts to deviate from that of the clean wing case and is referred to as the angle of activation. For the tested tubercle parameter ranges, as listed in TAB 3, the activation angle could be varied between 3° and 4.7°.

It is observed that streamwise vortices were formed either side of the tubercles which accelerated the flow in the trough region and resulted in delayed transition to a turbulent flow. For tubercles with a small leading edge radius, a laminar separation bubble (LSB) formed on the tubercle peak, see FIGURE 11 left. This resulted in a turbulent flow behind the peak and a laminar flow to be maintained for higher angles of attack behind the trough, resulting in an overall lower lift production after the activation angle in comparison to the D-form with a larger leading edge radius, see FIGURE 12. It is also observed that the drag is increased with a larger leading edge radius, with the sum of the drag within the drag bucket $c_{d,R}$ for the V-form being lower than that of the D-form, see FIGURE 12 and TAB 4. In the case of a larger leading edge radius and deeper valley at the trough, a greater flow attachment is

observed behind the peaks, see FIGURE 11 right. The formation of a LSB at lower angles of attack is prevented, therefore resulting in a larger region of laminar flow and a higher lift production compared to the *V*-form with a smaller radius, see FIGURE 12.
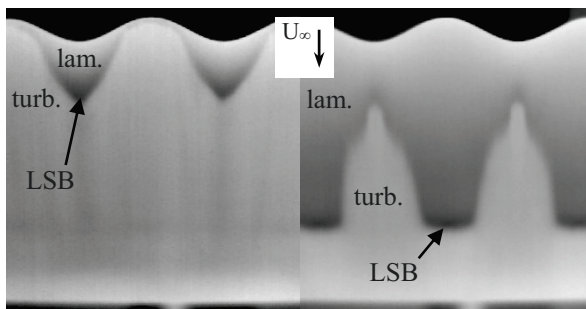

FIGURE 11. IRT flow visualization of the TEG4418 tubercle *V*-form (left) and *D*-form (right) with λ = 38%·*c* and *A* =7.5%·*c* for α = 6.0° and *Re* =8.06·10^5.
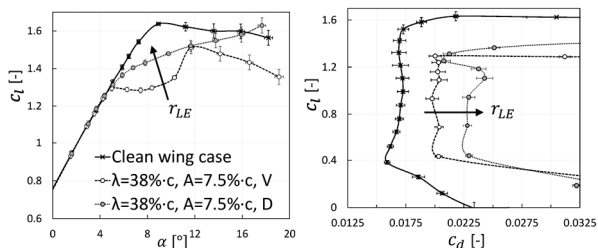

FIGURE 12. Measured lift and lift-drag polars for the TEG4418 at *Re* =8.06·10^5. Clean wing (solid line) and wing model with varying tubercle leading edge radius r_{LE}.

Tubercle Configuration	$C_{d,R}$ [-]	$C_{l,max}$ [-]	α_{act} [°]
λ=38%·*c*, *A*=5%·*c*, V	0.91	1.408	4.54
λ=38%·*c*, *A*=7.5%·*c*, V	0.84	1.293	4.24
λ=38%·*c*, *A*=7.5%·*c*, D	0.74	1.434	3.70
λ=38%·*c*, *A*=7.5%·*c*, Disc	0.99	1.342	4.69
λ=38%·*c*, *A*=10%·*c*, V	0.79	1.273	3.28
λ=19%·*c*, *A*=7%·*c*, V	0.84	1.364	3.01

TAB 4. Results for the tested tubercle configurations.

The findings, as shown in FIGURE 13, indicate that the wavelength has a significant influence on the activation angle, as vortices in closer proximity lead to the earlier onset of instability behind the troughs, as well as increasing the maximum lift with decreasing wavelength. The amplitude is observed to have a larger influence on the performance however, with an increased amplitude resulting in a larger drag increase and a decreased activation angle, see TAB 4. From FIGURE 13 it is also observed that a smaller amplitude results in a flatter lift curve after the activation angle.

By displacing the tubercles, creating a plateau at the trough with the *Disc*-form, it is observed that the neighboring counter-rotating vortices only interact and merge at higher angles of attack compared to the conventional *V*-form, see

FIGURE 15. This results in a larger region of laminar flow to be maintained behind the troughs and a smaller separated region at the trailing edge. The *Disc*-form thus results in a decreased lift production compared to the clean wing case with the resulting lift curve closely resembling that of the *V*-form tubercles. A minimal drag increase is however obtained with the use of the *Disc*-form, see FIGURE 14 and TAB 4.
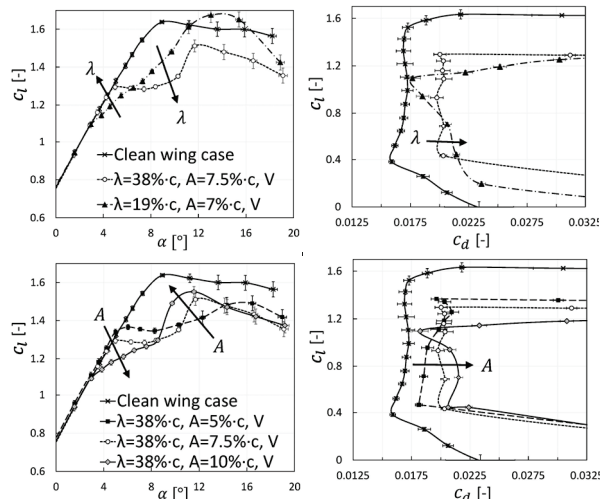

FIGURE 13. Measured lift and lift-drag polars for the TEG4418 at *Re* =8.06·10^5. Clean wing (solid line) and wing model with varied tubercle configurations for varying wavelength λ and amplitude *A*.
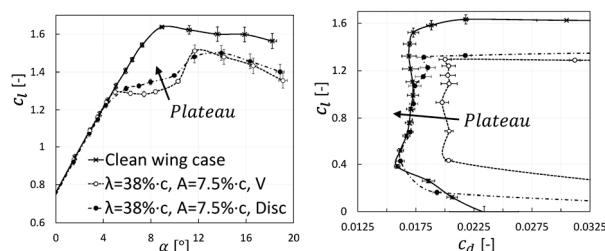

FIGURE 14. Measured lift and lift-drag polars for the TEG4418 at *Re* =8.06·10^5. Clean wing (solid line) and wing model with increased tubercle disc plateau.

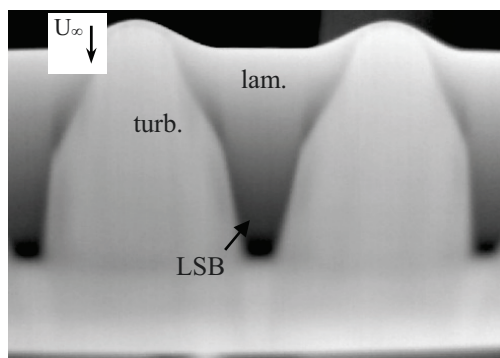FIGURE 15. IRT flow visualization of the TEG4418 tubercle Disc-form with λ =38%·*c* and *A*=7.5%·*c* for α = 6.2° and *Re* =8.06·10^5.

6. LEVOG RESULTS

With the parameter study, the LEVoG parameters are varied and the effects on the flow analyzed. The flow experiences an acceleration between the LEVoGs, resulting in delayed transition. As the LEVoG wake size increases and interacts with neighboring wakes downstream, the point of transition slowly creeps upstream with increasing angles of attack. It is observed that the implementation of LEVoGs maintains an attached flow on the front 19% of the wing at an angle of attack of $\alpha = 14°$, with the vortex streets behind the LEVoGs delaying separation up to appr. 58%, and coincides with that found in [19]. Thus the addition of the LEVoGs results in a lowered but maintained lift production with delayed separation.

Parameter ranges which produced the best results for the TEG4418 airfoil at a Reynolds number of $Re = 8.04 \cdot 10^5$ were identified for the LEVoG model configuration, relative to the airfoil chord length c, for a diameter $D = 1.71\% \cdot c$, height $H = 0.43\% \cdot c$, distance from the leading edge $s = 1.14\% \cdot c$ and spanwise spacing $S = 5.71\% \cdot c$, see FIGURE 16.
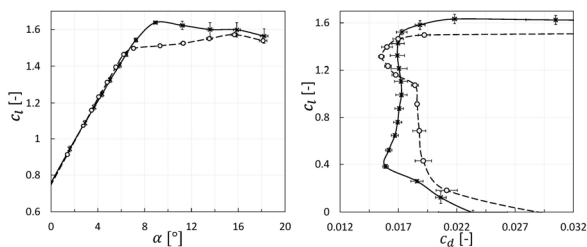

FIGURE 16. Measured lift and lift-drag polars for the TEG4418 at $Re =8.04 \cdot 10^5$. Clean wing (solid line) and wing model with LEVoG design D=1.71%·c, H=0.43%·c, s=1.14%·c and S=5.71%·c (dashed line).

It is observed that the addition of the LEVoGs does not affect the lift performance at lower angles of attack. The addition of the LEVoGs results in a higher overall drag coefficient but experiences a decrease in drag when located in or near the stagnation point. For the optimum LEVoG configurations the drag is observed to be lower than the clean airfoil case for a narrow incidence range pre-LEVoG activation. This effect is attributed to the larger influence of the laminar separation bubble (LSB) at lower Reynolds numbers. Furthermore, it is concluded that due to the difference in the position of the stagnation point for different airfoils, the LEVoG activation angle is affected and is attributed to the local boundary layer thickness δ. Due to the large influence of the LEVoG parameters, the activation angle could be varied between 3° and 7° with a 7.3% reduction of the maximum lift.

Of the LEVoG parameters, the LEVoG distance from the leading edge s as well as height H were found to have the largest influence on the aerodynamic performance. Both influenced the ratio of the LEVoG height to boundary layer thickness H/δ. The boundary layer thickness δ was numerically calculated using XFOIL for the TEG4418 clean airfoil with a Reynolds number $Re = 8.05 \cdot 10^5$, Mach number $Ma = 0.11$ and critical amplification factor used by XFOIL of $Ncrit = 8$. With an increase in the ratio H/δ, a decrease in the maximum lift was observed, see FIGURE 17. However,

this also resulted in an increased drag, specifically at lower angles of attack pre-activation and was assumed to be due to the larger LEVoG wake height experienced on the model lower surface. From the results the optimum ratio of LEVoG height to boundary layer thickness was found to lie within the range $2 < H/\delta < 5$.

An optimum ratio of the LEVoG spanwise spacing to diameter S/D was also observed as a reduced effective spacing between the LEVoGs S_{eff}, affected by both the spanwise spacing S and diameter D, resulted in a significantly increased drag, as illustrated in FIGURE 18 for varying S_{eff}. An increase in the effective spacing does not have a significant effect on the lift curve, only slightly increasing the lift post-activation. The optimum ratio, which resulted in the lowest increase in drag as well as a flatter lift curve, was identified for the spacing ratio range between $2.8 < S/D < 5.0$.
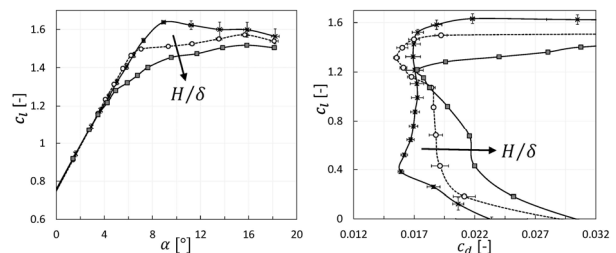

FIGURE 17. Measured lift and lift-drag polars for the TEG4418 at $Re =8.04 \cdot 10^5$. Clean wing (solid line) and wing model with varied LEVoG configurations for the ratio of the height to boundary layer thickness H/δ.

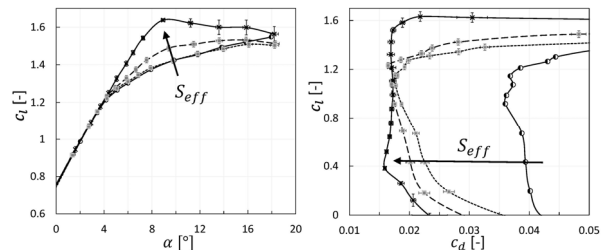
FIGURE 18. Measured lift and lift-drag polars for the TEG4418 at $Re =8.04 \cdot 10^5$. Clean wing (solid line) and wing model with varied LEVoG configurations for the ratio of the effective spacing S_{eff}.

In order to compare the results of the various LEVoG modifications, a few analysis criteria were chosen and analyzed with the use of contour plots. These criteria were: The angle of attack at which the lift production deviates from the clean wing case, referred to as the activation angle α_{act}, the gradient of the lift curve after activation a, the maximum lift $c_{l,max}$ as well as the ratio of the sum of the drag within the drag bucket of the tested model configuration to that of the clean wing case $c_{d,R}$.

From the results of all the tested LEVoG configurations for a Reynolds number $Re = 8.05 \cdot 10^5$, all generated contour plots were thus analyzed. However, since the form of the Reynolds number as well as the implemented profile for future applications can vary to that of the tested TEG4418

airfoil, thus changing the exact location of the stagnation point and the boundary layer thickness, it is not possible to define the exact parameters which will produce the optimum results. Optimum parameter ranges for the LEVoG height H, distance to the leading edge s, spacing S and diameter D as well as the previously defined ratios H/δ and S/D, were therefor identified, shown in white in FIGURE 19 and FIGURE 20. Using these contour plots, a better approximation of the needed parameters can thus be obtained.
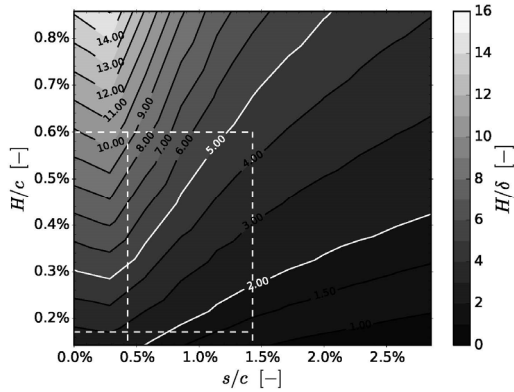

FIGURE 19. Resulting optimum LEVoG parameter ranges for the LEVoG height H, distance to the leading edge s and ratio of the LEVoG height to boundary layer thickness H/δ, given in percent chord $\% \cdot c$.
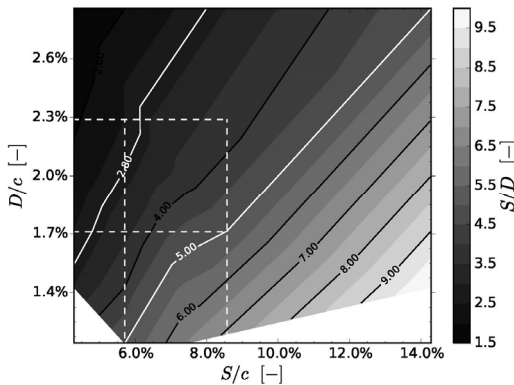

FIGURE 20. Resulting optimum LEVoG parameter ranges for the LEVoG diameter D and spanwise spacing S to the spacing ratio S/D, given in percent chord $\% \cdot c$.

7. DISCUSSION

The findings of the tubercle amplitude and wavelength variation are consistent with that observed in previous research. The observed flow characteristics for the tubercles are also in line with the results described in [22], [23] and [24]. It should be noted that in previous research, as observed in [20] and [21], it was found that the tubercle effectiveness reduced with a decrease in the Reynolds number, as this resulted in an increased drag. It can therefore be expected that the observed drag penalty for the current application should be reduced when tested at higher Reynolds numbers.

From the results it is observed that the use of tubercles does offer a promising solution to limit the lift production beyond the activation angle. Implementing an increased plateau between tubercles was found to reduce the lift with a minimal drag penalty. Variation of the tubercle parameters however, does not allow significant adjustment of the activation angle, thus limiting the adjustability to that of the wind power plant's operation point.

The implementation of LEVoGs does offer a larger variation of the activation angle, due to the larger influence of the various LEVoG parameters on the aerodynamic performance thus offering better adjustability for a specific application. A flatter lift curve after activation is however only possible with a higher activation angle, which in turn only offers a small reduction of the maximum lift. The addition of the LEVoGs result in a higher overall drag coefficient, but was observed to experience a decrease in drag when the LEVoGs are located in or near the stagnation point. Depending on the LEVoG distance from the leading edge, the angle of attack at which the LEVoGs are activated can be influenced.

The ratio of the LEVoG height to boundary layer thickness is found to be a driving factor, with the optimum ratio for the current application found to lie between 2 and 5. This differs from the ratio of appr. 1 suggested in [25] for improved dynamic-stall conditions. Furthermore, it was found that an optimum ratio for the spacing to diameter S/D exists, contradicting the conclusion in [17] which stated that the spacing only has a weak influence on the aerodynamic performance. The spacing ratio range, which results in the lowest drag increase and a flatter lift curve, was defined for the range 2.8 to 5.

The generated contour plots from the LEVoG results, illustrated in FIGURE 19 and FIGURE 20, should offer a better approximation when designing LEVoGs for similar applications to obtain a reduced lift production beyond the designed operation point, such as that defined in FIGURE 1.

8. CONCLUSION AND OUTLOOK

The first part of this work focused on the preparation and improvement of the UniBwM wind tunnel to investigate and develop wing airfoils. The acquisition of an airfoil polar now takes less than 1h including model exchange and the results show very good coincidence with the reference data. Therefore it was decided to continue with the investigation of leading edge modification of wind turbine airfoils to improve the characteristics with respect to limited high lift loading.

Experimental results are presented for the implementation of sinusoidal leading edge tubercles and Leading Edge Vortex Generators (LEVoGs) on laminar, wind turbine airfoils TEG4418 and TEG2618 at a testing Reynolds number of Re=0.8·10[6]. The measured lift and drag polars, infra-red thermography and oil flow visualization are used for the investigation of the flow and the parameter analysis. The results from the analysis of the tubercle and LEVoG parameter variation are consistent with that observed in previous research.

The findings suggest that both tubercles and LEVoGs can be implemented to lower the lift production beyond the operation point for use in wind power plants. The use of LEVoGs however, offers larger design flexibility in comparison to that of tubercles. Additionally, this research offers a better understanding of the effect of the tubercle and LEVoG parameters on the resulting aerodynamic performance. Future investigations at higher Reynolds numbers are necessary to determine whether, and to what degree, the effect of the LEVoGs changes with an increased Reynolds number.

ACKNOWLEDGEMENTS

REFERENCES

[1] F.E. Fish and J. M. Battle, ''Hydrodynamic design of the humpback whale flipper,'' Journal of Morphology 225, 51, 1995.

[2] D.S. Miklosovic, M.M. Murray, L.E. Howle and F.E. Fish, "Leading-Edge Tubercles Delay Stall on Humpback Whale (Megaptera novaeangliae) Flippers," *Physics of Fluids*, **16**, (5), pp. L39-L42, 2004.

[3] D.S. Miklosovic, M.M. Murray and L.E. Howle, "Experimental Evaluation of Sinusoidal Leading Edges", Journal of Aircraft, Vol. 44, No. 4, July–August 2007

[4] H. Johari, C. Henoch, D. Custodio and A. Levshin, "Effects of Leading Edge Protuberances on Airfoil Performance", AIAA Journal Vol. 45, No. !!, 2007.

[5] E.A. van Nierop, S. Alben and M.P. Brenner, „How Bumps on Whale Flippers Delay Stall: An Aerodynamic Model", Physical Review Letters, PRL 100, 054502, 2008

[6] K.L. Hansen, "Effect of Leading Edge Tubercles in Airfoil Performance", Thesis, The Univ. of Adelaide, 2012

[7] N. Rostamzadeh, R. M. Kelso, B. Dally, "A numerical investigation into the effects of Reynolds number on the flow mechanism induced by a tubercled leading edge", Theor. Comput. Fluid Dyn., Springer, 2016

[8] A.F.A. Gawad, "Utilization of Whale-Inspired Tubercles as a Control Technique to Improve Airfoil Performance", Transaction on Control and Mechinal Systems, Vol. 2, No. 5, pp. 212-218, 2013

[9] SAE, "Aerodynamic testing of road vehicles in open jet wind tunnels", SP-1465. Society of Automotive Engineers, 1999

[10] C. Eder, "Optimierung des Druckgradienten im großen Windkanal durch Optimierung des Kollektors" Master's thesis. Universität der Bundeswehr München, 2015

[11] T. Terreblanche, "Optimization of Profile Polars for Wind Turbine Rotor Blades with the use of Leading-Edge Vortex Generators", Master's Thesis, TU Braunschweig, 2017

[12] W. Wuest, "Strömungsmeßtechnik", Vieweg & Sohn GmbH, Braunschweig, p47, 1969

[13] B.M. Jones, "The Measurement of Profile Drag by the Pitot-traverse Method", Cambridge University Aeronautics Laboratory, Aeronautical Research Council (Great Britain), Air Ministry, H.M. Stationery Office, 1936

[14] W. Nitsche and A. Brunn, „Strömungsmess-technik", Springer Berlin Heidelberg, p16, 2006.

[15] M. Drela and H. Youngren, "XFOIL 6.9: General Description", Cambridge USA

[16] W. Geissler, G. Dietz, H. Mai, and H. Richard, "Dynamic Stall and its Passive Control Investigations on the OA209 Airfoil Section." In: 31th European Rotorcraft Forum. Vol. 41, p1-14, 2005

[17] H. Mai, G. Dietz, W. Geissler, K. Richter, J. Bosbach, H. Richard and K. Groot. "Dynamic Stall Control by Leading Edge Vortex Generators." In: Journal of the American Helicopter Society 53.1 p. 26, 2008

[18] B. Heine, K. Mulleners, G. Joubert, and M. Raffel. "Dynamic Stall Control by Passive Disturbance Generators." In: AIAA Journal 51.9, pp. 2086–2097, 2013

[19] B. Heine, T. Schwermer and M. Raffel, "The effect of vortex generators on the flow around a circular cylinder". In: 15th International Symp. on Applications of Laser Techniques to Fluid Mechanics, Göttingen, 2010

[20] H. Johari, C.W. Henoch, D. Custodio and A. Levshin, "Effects of Leading-Edge Protuberances on Airfoil Performance." In: AIAA Journal 45.11, pp. 2634–2642, 2007

[21] Hansen, K. L., Kelso, R. M., and Dally, B. B. "An investigation of three-dimensional effects on the performance of tubercles at low Reynolds numbers." In: Proceedings of 17th Australasian Fluid Mechanics Conference. Red Hook, NY: University of Auckland, 2010.

[22] M. Zhao, M. Zhang and J. Xu, "Numerical simulation of flow characteristics behind the aerodynamic performances on an airfoil with leading edge protuberances." In: Engineering Applications of Computational Fluid Mechanics 11.1 pp. 193–209, 2017

[23] A. Skillen, A. Revell, A. Pinelli, U. Piomelli and J. Favier, "Flow over a Wing with Leading-Edge Undulations." In: AIAA Journal 53.2 pp. 464–472, 2015

[24] M.W. Lohry, D. Clifton and L. Martinelli, "Characterization and Design of Tubercle Leading-Edge Wings." In: 7th International Conference on Computational Fluid Dynamics, Vol. ICCFD7-4302, 2012

[25] B. Heine, "Passive Beeinflussung von Dynamic Stall durch Störgeneratoren." Doktor-Ingenieur. Hannover: Gottfried Wilhelm Leibnitz Universität, 2012.